January 2015

Ball-milled FeP/graphite as a low-cost anode material for the sodium-ion battery

Qiuran Yang
University of Wollongong, qy877@uowmail.edu.au

Weijie Li
University of Wollongong, wl347@uowmail.edu.au

Shulei Chou
University of Wollongong, shulei@uow.edu.au

Jiazhao Wang
University of Wollongong, jiazhao@uow.edu.au

Hua-Kun Liu
University of Wollongong, hua@uow.edu.au

Ball-milled FeP/graphite as a low-cost anode material for the sodium-ion battery

Abstract

Phosphorus is a promising anode material for sodium batteries with a theoretical capacity of 2596 mA h g^{-1}. However, phosphorus has a low electrical conductivity of 1 x 10^{-14} S cm^{-1}, which results in poor cycling and rate performances. Even if it is alloyed with conductive Fe, it still delivers a poor electrochemical performance. In this article, a FeP/graphite composite has been synthesized using a simple, cheap, and productive method of low energy ball-milling, which is an efficient way to improve the electrical conductivity of the FeP compound. The cycling performance was improved significantly, and when the current density increased to 500 mA g^{-1}, the FeP/graphite composite could still deliver 134 mA h g^{-1}, which was more than twice the capacity of the FeP compound alone. Our results suggest that by using a low-energy ball-milling method, a promising FeP/graphite anode material can be synthesized for the sodium battery.

Keywords

low, ball, milled, fep, cost, anode, material, battery, ion, graphite, sodium

Publication Details

Yang, Q., Li, W., Chou, S., Wang, J. & Liu, H. (2015). Ball-milled FeP/graphite as a low-cost anode material for the sodium-ion battery. RSC Advances: an international journal to further the chemical sciences, 5 (98), 80536-80541.

RSC Advances

PAPER

View Article Online
View Journal | View Issue

Cite this: *RSC Adv.*, 2015, **5**, 80536

Ball-milled FeP/graphite as a low-cost anode material for the sodium-ion battery

Qiu-Ran Yang, Wei-Jie Li, Shu-Lei Chou,* Jia-Zhao Wang and Hua-Kun Liu

Received 29th July 2015
Accepted 9th September 2015

DOI: 10.1039/c5ra18314f

www.rsc.org/advances

Phosphorus is a promising anode material for sodium batteries with a theoretical capacity of 2596 mA h g^{-1}. However, phosphorus has a low electrical conductivity of 1×10^{-14} S cm^{-1}, which results in poor cycling and rate performances. Even if it is alloyed with conductive Fe, it still delivers a poor electrochemical performance. In this article, a FeP/graphite composite has been synthesized using a simple, cheap, and productive method of low energy ball-milling, which is an efficient way to improve the electrical conductivity of the FeP compound. The cycling performance was improved significantly, and when the current density increased to 500 mA g^{-1}, the FeP/graphite composite could still deliver 134 mA h g^{-1}, which was more than twice the capacity of the FeP compound alone. Our results suggest that by using a low-energy ball-milling method, a promising FeP/graphite anode material can be synthesized for the sodium battery.

Introduction

Due to the increasing demand for consumer electronic devices and electric vehicles every year, and the severe environmental problems that are brought about by the use of traditional automobiles, development of high-energy storage devices has become a crucial issue.[1] Using lithium-ion batteries is an essential way to solve this issue,[2] but lithium resources are not sufficient for widespread use. Because of the similarities in chemical properties between sodium and lithium, the sodium-ion battery has become the most available substitute for the lithium battery.[3] There are a variety of Na-ion anode materials, such as hard carbon,[4] metal oxides,[5] and metals which can alloy with sodium.

Tin (847 mA h g^{-1}), antimony (664 mA h g^{-1}), and phosphorus (2560 mA h g^{-1}) are attractive anode materials because of their high theoretical capacity. According to Qian's[6] report, the electrical conductivity and volume changes during cycling significantly affect the performance of alloy compounds. Coating carbon or using carbon material as matrix are efficient methods to improve cycle life and rate performances in alloy anodes. For example, in Zhu's group,[7] wood fiber was found to work as a mechanical buffer, and after 400 cycles, the retained capacity was around 339 mA h g^{-1}, 40% of the initial capacity. Wang's group[8] prepared Sn@carbon nanotube composite delivering a capacity of 550 μA h cm^{-2} in the 100th cycle, which was 62% of the initial cycle. Ji *et al.*[9] prepared an Sb/acetylene black composite which delivered a capacity of 73 mA h g^{-1} after 70 cycles, with initial capacity of 624 mA h g^{-1}. Wu *et al.*[10] synthesized Sb@C microspheres with 93% capacity retention after 100 cycles. P has a high theoretical capacity of 2596 mA h g^{-1} in sodium battery. However, phosphorus has a low electrical conductivity of 1×10^{-14} S cm^{-1}, which results in poor cycling and rate performances. One efficient way is to synthesize P/carbon composites. Kim and Qian[11] separately reported a phosphorus/C composite to achieve high cycling stability. Inspired by this, our group[12] prepared a red phosphorus/carbon nanotube (CNT) composite by simply hand grinding, which retained 76.6% of the initial capacity in the 10th cycle.

Our group[13] has studied iron phosphide (FeP) compound for application in sodium batteries, as it has high initial capacity of over 700 mA h g^{-1}. The capacity of a sample with poly(vinylidene difluoride) (PVDF) binder decreased to around 50 mA h g^{-1} after 40 cycles, because of the poor electrical conductivity. One efficient way to improve the FeP compound is to use carbon material to make a composite.

According to previous report, ball milling is a cheap and productive way to synthesis carbon coated composite.[14] Our group's previous works[13,15] demonstrate that after 20 hours milling at the rotation speed of 300 rpm can get the nanoparticles about 30–100 nm in size which can deliver well electrochemical performance. Based on our previous experience, FeP/graphite composite was prepared by this ball milling method at optimized condition. After that, graphite turns into an amorphous carbon matrix with FeP particles embedded in it. The amorphous carbon serves as a conductive and ductile matrix to connect particles with improved electrical conductivity and to buffer the volume change, which significantly improves the cycling and rate performances. FeP/graphite will be a promising anode material in the future.

Institute for Superconducting and Electronic Materials, University of Wollongong, Wollongong, NSW 2522, Australia. E-mail: shulei@uow.edu.au

Experiment section

Synthesis of FeP/graphite composite

FeP/graphite composite was synthesis by a simple and productive low-energy ball-milling method. FeP/graphite composite powder was prepared by using FeP compound and commercial graphite. The FeP compound and graphite were mixed in the weight ratio of 7 : 3, respectively and then put into a hardened steel vial with 2 mm diameter milling balls. The weight ratio of balls to powder was 20 : 1. The vial was assembled in a glove box with water and oxygen lower than 0.1 ppm. The rotation conditions were set to 300 rpm for 20 hours.

Characterization

The crystal structure was characterized by X-ray diffraction (XRD). The XRD patterns of the as-prepared powders were collected on a GBC MMA instrument with a Cu K_α source (λ = 1.541 Å), operating at 40 kV and 25 mA (step size = 0.002° s^{-1}). Scanning electron microscopy (JEOL JSM-7500FA) and transmission electron microscopy (TEM, JEOL 2011, 200 keV) were used to characterize the morphology of the samples. Raman spectra were collected using a HR800 JOBIN Yvon Horiba Raman spectrometer.

Electrochemical measurements

In order to evaluate the electrochemical performance, the FeP/graphite and FeP electrodes were prepared by mixing 80 wt% active material, 10 wt% carbonyl-β-cyclodextrin, and 10 wt% carbon black with de-ionised (DI) water to form a homogeneous slurry, which was then coated on Cu foil, dried at 80 °C for 10 hours in a vacuum oven, and then pressed under a pressure of 10 MPa. The electrodes were then punched into disks with 3 mg cm^{-2} active material loaded on them. The electrolyte was $NaClO_4$ in a mixture of ethylene carbonate (EC) and diethyl carbonate (DEC) in the ratio of 1 : 1 by volume. The cell was assembled in an Ar-filled glove box with water and oxygen content lower than 0.1 ppm. The assembled cells were tested on a Land cycler (Wuhan) at the current density of 50 mA g^{-1} within the voltage window of 0–1.5 V (*vs.* Na/Na^+). C-rate tests were conducted under current densities from 50 mA g^{-1} to 2500 mA g^{-1} within the voltage range of 0–1.5 V (*vs.* Na/Na^+).

Results and discussion

Fig. 1(a) shows the XRD patterns of FeP/graphite and pure FeP compound. All the diffraction peaks are indexed to orthorhombic phase (JPCDS no. 65-2595) with space group *Pnma*. The decreased peak intensity of FeP/graphite compared to the original FeP is due to the smaller grain size after 20 hours of low energy ball milling. Based on the Debye–Scherrer[16] formula, $D = K\gamma/(B\cos\theta)$, K is a numerical factor referred to as the crystallite-shape factor, γ is the wavelength of the X-ray, B is the half maximum width of X-ray peak and θ is Bragg angle. After calculating, the FeP crystal size in FeP/graphite was calculated about 14.5 nm.

In order to further analyze the structure of FeP/graphite composite, Raman spectroscopy was carried out. As shown in Fig. 1(b), the Raman spectrum of FeP/graphite has two obvious bands at 1330 cm^{-1} and 1570 cm^{-1}, corresponding to the D and G bands of carbon, respectively. The D band assigned to the A_{1g} mode corresponds to the defects in the structure, and the G band is assigned to the first-order scattering of the E_{2g} mode in the graphitic structure.[6,17] The intensity ratio of D/G (I_D/I_G) characterizes the ratio of disordered to ordered carbon in the sample. The intensity ratio from the spectrum for pure graphite is 0.28, while the I_D/I_G ratio of FeP/graphite is 1.18. This phenomenon indicates that the graphite has been transformed to disordered carbon after 20 hours of ball milling, which is consistent with the XRD pattern, where no graphite peak can be observed. There are no significant Fe–P bands in the spectrum, which indicates that the FeP particles might be covered with amorphous carbon. In addition, there is no band for P–P or P–C, and no obviously peak shifting can be observed, which indicates that the FeP compound has not decomposed or reacted with graphite after ball milling.

To explore the morphology of FeP/graphite after ball milling, scanning electron microscopy (SEM) and energy dispersive spectroscopy (EDS) mapping were conducted. Fig. 2(a) and (b) show the surface morphology of FeP compound and FeP/graphite composite powder after 20 hours of ball milling.

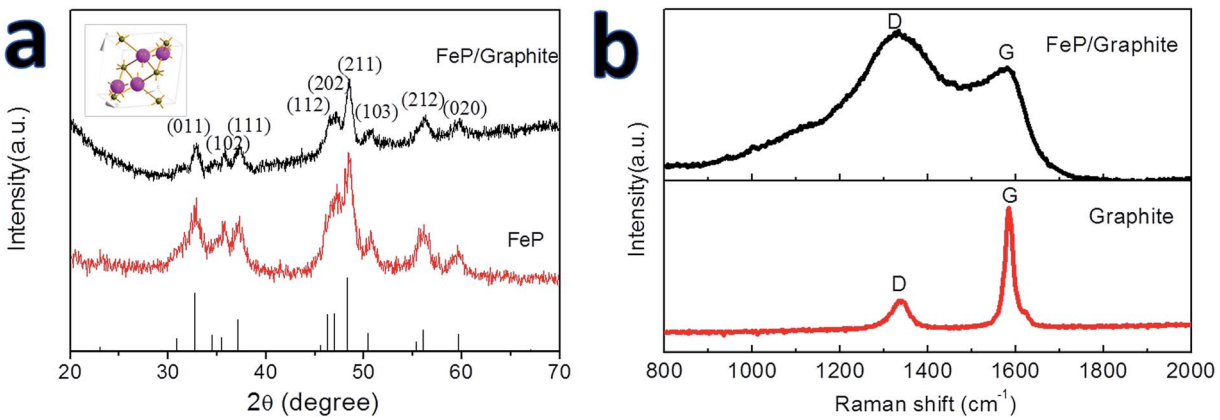

Fig. 1 (a) XRD patterns of FeP/graphite and FeP, and (b) Raman spectra of FeP/graphite composite and graphite.

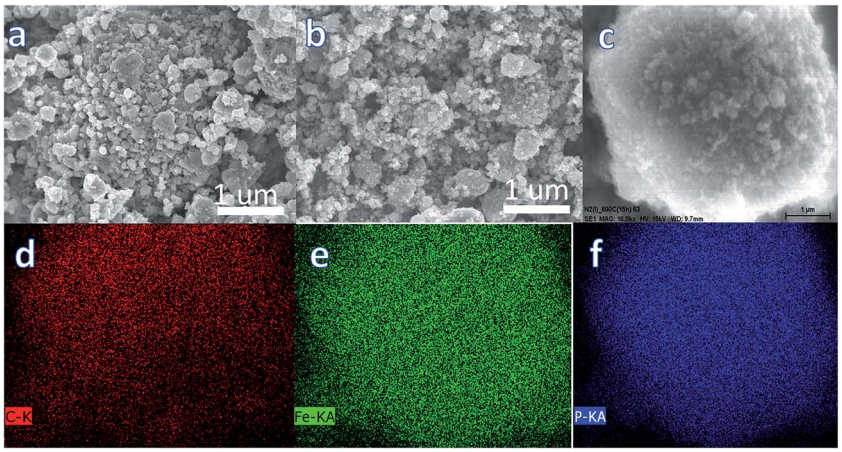

Fig. 2 SEM images of FeP compound (a) and FeP/graphite composite (b and c); (d–f) are the EDS mapping of the FeP/graphite composite particle in (c).

Compared to the original FeP compound, the average size of secondary particles in the FeP/graphite composite is decreased from 100–150 nm to about 100 nm, which is consistent with the decreased peak intensity in the XRD pattern. The irregular-shaped original particles have become spherical, which is advantageous for battery application. In order to confirm that the FeP was mixed homogeneously with the carbon, an individual particle in Fig. 2(b) was explored by EDS mapping, as shown in Fig. 2(c). It seems that the carbon was distributed homogeneously over the FeP compound particles, which is in accordance with the Raman result that no Fe–P or P–P band could be observed.

To further confirm that the FeP compound particles were embedded in amorphous carbon, transmission electron microscopy (TEM) and selected area electron diffraction (SAED) analysis (Fig. 3) were conducted on the as-prepared composite powder. In Fig. 3(a), lattice fringes with *d*-spacing of 0.273 nm, corresponding to the (011) planes of FeP, are observed. There are no lattice fringes between the FeP and the amorphous carbon, which indicates that no bonding was formed between the FeP and the carbon,[18] which is in line with the Raman spectra. The FeP nanocrystals are embedded in the amorphous carbon matrix. The electron diffraction rings, corresponding to the (011), (211), and (103) planes of FeP, are shown in Fig. 3(b). Combining the evidence above, it is clear that, after simple ball milling, the graphite is converted to amorphous carbon with FeP crystalline particles 10 nm in size homogeneously embedded inside. The amorphous carbon can serve as a conductive matrix to enable well electric contact between particles so that can improve the cycling and rate performance.

As shown in Fig. 4, transmission electron microscopy (TEM) and selected area electron diffraction (SAED) analysis were used to analyze the structure and phase of FeP and FeP/graphite electrodes after cycling for two cycles and charged at 1.5 V. The electron diffraction patterns of FeP and FeP/graphite are similar. The electron diffraction rings are corresponding to (101), (100), (004), (103) phase of polycrystal Fe, which indicate that after one cycle FeP might has decomposed into Fe and amorphous P which is in accordant with the previous report.[13] As can be seen from the TEM image in Fig. 4(a), after cycling FeP electrode particles have pulverized into small nanoparticles, and isolated which results in poor cycling and rate

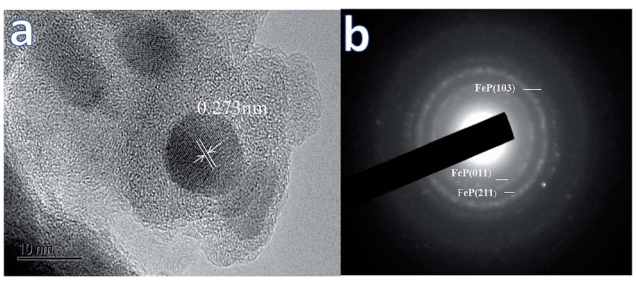

Fig. 3 TEM image (a) and SAED pattern (b) of FeP/graphite composite.

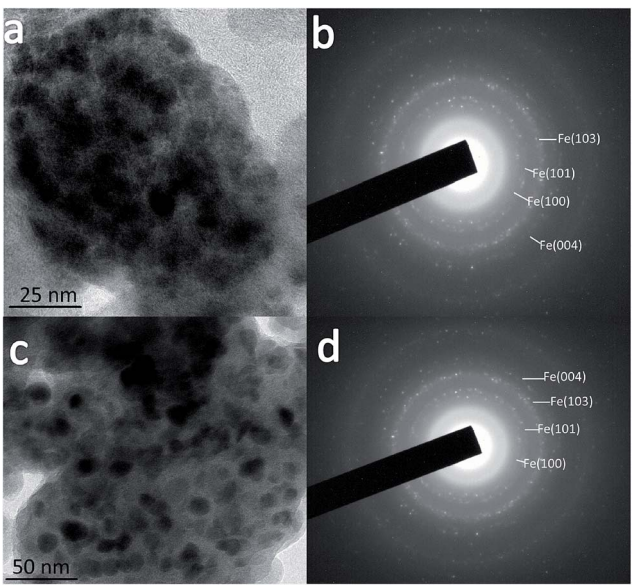

Fig. 4 TEM (a and c) and SEAD (b and d) images of FeP (a and b) and FeP/graphite (c and d) electrodes charged at 1.5 V.

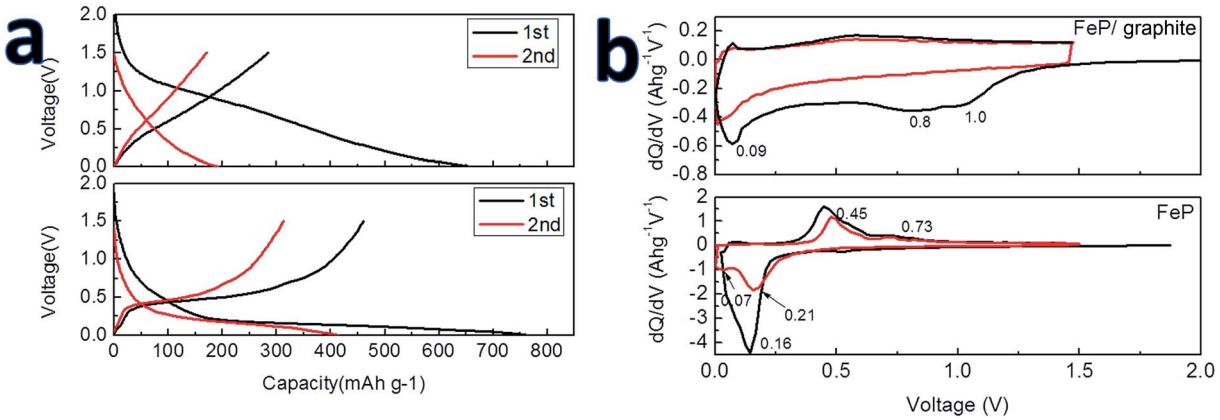

Fig. 5 Charge–discharge curves at the current density of 50 mA g^{-1} (a) and corresponding dQ/dV plots (b) in the first two cycles for FeP/graphite (top) and FeP (bottom) electrodes.

performance. Comparing to FeP electrode, the FeP/graphite (Fig. 4(b)) electrode has Fe particles imbedded in the amorphous carbon, thus amorphous carbon can serve as conductive matrix to maintain the good electrical contact between particles and hinder pulverization during cycling.

The discharge and charge performances of de-alloying and alloying of Na-ion with FeP compound and FeP/graphite composite was examined in 1.0 mol L^{-1} $NaClO_4$ in EC–DEC solution (1 : 1 v/v). The loading mass of active material was ~3 mg cm^{-2}. Fig. 4(a) displays the discharge and charge profiles (within the voltage range of 0–1.5 V *vs.* Na/Na^+) of FeP compound and FeP/graphite under the current density of 50 mA g^{-1}. The discharge capacity of FeP/graphite composite in the first cycle is 658.4 mA h g^{-1}. The calculated specific capacity based on the ratio of FeP compound is 823 mA h g^{-1}, which is close to the theoretical capacity of 893.3 mA h g^{-1} and higher than the pure FeP capacity of 764.5 mA h g^{-1}. During the initial discharge of FeP/graphite, a slope between 0.8–1.0 V can be clearly observed, which corresponds to the formation of the solid electrolyte interphase (SEI). The plateau at 0.09 V is similar to that of FeP compound, which is due to Na alloying with P to form Na_3P.[13]

In order to compare the chemical reactivity of the FeP/graphite composite to FeP compound, and to analysis the mechanism of in both samples, differential capacity (dQ/dV) curves were plotted, as shown in Fig. 4(b). In the first discharge process, two cathodic peaks are observed, *i.e.*, one wide peak (0.8–1.0 V *versus* Na/Na^+) and one sharp peak (0.09 V *versus* Na/Na^+). The first wide current cathodic peak can be ascribed to the decomposition of electrolyte and the formation of the SEI. The second small peak is assigned to the alloy step of sodium ion insertion reaction to form Na_3P and NaC_x.[19] It is obviously observed an anodic peak at 0.05 V which corresponds to the desodiation. The overall reaction process can be summarized as follows:

$$3Na^+ + 3e^- + Fe + P \leftrightarrow Na_3P + Fe \quad (1)$$

$$xC + Na^+ + e^- \leftrightarrow NaC_x \quad (2)$$

The dQ/dV curve of FeP compound plotted in Fig. 4(b) shows that there are two cathodic peaks at 0.07 V and 0.21 V, and two anodic peaks at 0.44 V and 0.76 V in the second cycle, which is similar to the reported curve.[13] These peaks correspond to the alloying and de-alloying reactions between Na^+ and FeP compound.

Fig. 5(a) shows the cycling performances of FeP/graphite and FeP compound. The discharge capacity of FeP at the 70th cycle is

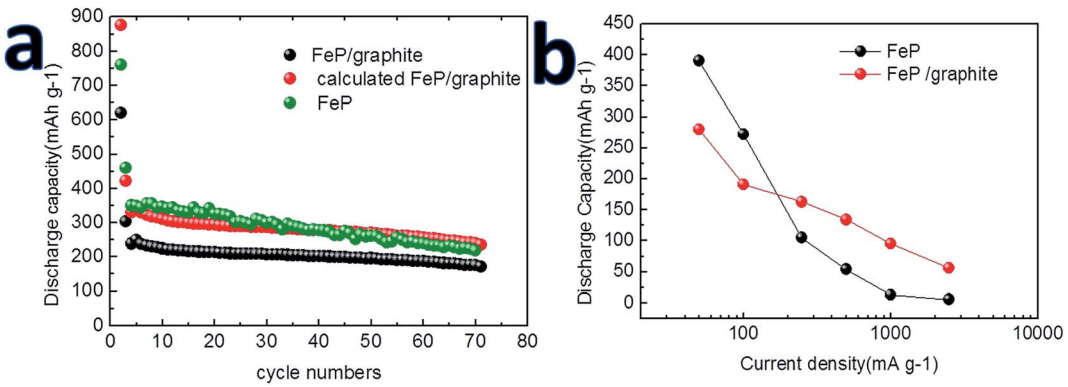

Fig. 6 Cycling performances of FeP/graphite, calculated FeP/graphite, and FeP compound (a) at 50 mA g^{-1}. Rate performance of FeP compound and FeP/graphite composite (b).

217 mA h g^{-1}, which represents 47% capacity retention with respect to the second cycle. The FeP/graphite composite shows an obvious improvement in cycling performance. The 70th discharge capacity is 175 mA h g^{-1}, which is 58% of the second cycle. The reason for the lower capacity of FeP/graphite compared to FeP is the limited specific capacity of graphite. If the capacity is calculated based on the weight of FeP only, after 70 cycles, the capacity remains 240 mA h g^{-1}, which is higher than that of pristine FeP. The main reason for the improvement in cycling performance is that the amorphous carbon can connect the isolated particles and improve the electrical conductivity. Fig. 5(b) shows the rate capabilities of FeP and FeP/graphite electrodes. The average discharge capacities are 390/280, 272/191, 105/163, 54/134, 13/95, and 5.5/56 mA h g^{-1} at current densities of 50, 100, 250, 500, 1000, and 2500 mA g^{-1} for the FeP and FeP/graphite electrodes, respectively. It is obvious that the rate capacity of FeP/graphite is better than that of FeP, especially when the current density increases to over 500 mA g^{-1}. This is probably because the amorphous carbon can serve as conductive matrix to maintain the contact between particles and hinder pulverization during cycling (Fig. 6).

Conclusion

In summary, FeP/graphite composite was prepared by a simple low-energy ball-milling method. The results demonstrate that, after ball milling with graphite, the cycling and high-rate performances of FeP compound were greatly improved: the discharge capacity of FeP/graphite represents 58% capacity retention with respect to the second cycle; when the current density increased to 500 mA g^{-1}, FeP/graphite composite still delivered 134 mA h g^{-1}, which was more than twice the capacity of the FeP compound. The graphite was converted to amorphous carbon after ball milling, which served as a conductive matrix to well connect the particles, hinder pulverization and improve the electrical conductivity. Our results suggest that FeP/graphite composite will be a cheap and productive anode material for sodium ion batteries in the future.

Acknowledgements

This work is supported by the Australian Research Council through a Linkage Project (LP120200432). The authors would like to also thank Dr Tania Silver for critical reading of the manuscript, and also acknowledge the use of the facilities in the UOW Electron Microscopy Centre, with particular thanks to Dr Gilberto Casillas-Garcia.

References

1 Z. Yang, J. Zhang, M. C. Kintner-Meyer, X. Lu, D. Choi, J. P. Lemmon and J. Liu, Electrochemical energy storage for green grid, *Chem. Rev.*, 2011, **111**(5), 3577–3613.

2 (*a*) M. S. Whittingham, Lithium batteries and cathode materials, *Chem. Rev.*, 2004, **104**(10), 4271–4302; (*b*) W.-J. Zhang, A review of the electrochemical performance of alloy anodes for lithium-ion batteries, *J. Power Source*, 2011, **196**(1), 13–24.

3 (*a*) V. Palomares, P. Serras, I. Villaluenga, K. B. Hueso, J. Carretero-González and T. Rojo, Na-ion batteries, recent advances and present challenges to become low cost energy storage systems, *Energy Environ. Sci.*, 2011, **5**(3), 5884–5901; (*b*) B. L. Ellis and L. F. Nazar, Sodium and sodium-ion energy storage batteries, *Curr. Opin. Solid State Mater. Sci.*, 2012, **16**(4), 168–177; (*c*) A. Ponrouch, R. Dedryvère, D. Monti, A. E. Demet, J. M. A. Mba, L. Croguennec, C. Masquelier, P. Johansson and M. R. Palacín, Towards high energy density sodium ion batteries through electrolyte optimization, *Energy Environ. Sci.*, 2013, **6**(8), 2361–2369; (*d*) M. D. Slater, D. Kim, E. Lee and C. S. Johnson, Sodium-Ion Batteries, *Adv. Funct. Mater.*, 2013, **23**(8), 947–958; (*e*) Y. Kim, K. H. Ha, S. M. Oh and K. T. Lee, High-Capacity Anode Materials for Sodium-Ion Batteries, *Chem.–Eur. J.*, 2014, **20**(38), 11980–11992; (*f*) N. Yabuuchi, K. Kubota, M. Dahbi and S. Komaba, Research development on sodium-ion batteries, *Chem. Rev.*, 2014, **114**(23), 11636–11682.

4 (*a*) A. Ponrouch, A. R. Goñi and M. R. Palacín, High capacity hard carbon anodes for sodium ion batteries in additive free electrolyte, *Electrochem. Commun.*, 2013, **27**, 85–88; (*b*) J. Zhao, L. Zhao, K. Chihara, S. Okada, J.-I. Yamaki, S. Matsumoto, S. Kuze and K. Nakane, Electrochemical and thermal properties of hard carbon-type anodes for Na-ion batteries, *J. Power Source*, 2013, **244**, 752–757; (*c*) M. Dahbi, T. Nakano, N. Yabuuchi, T. Ishikawa, K. Kubota, M. Fukunishi, S. Shibahara, J.-Y. Son, Y.-T. Cui, H. Oji and S. Komaba, Sodium carboxymethyl cellulose as a potential binder for hard-carbon negative electrodes in sodium-ion batteries, *Electrochem. Commun.*, 2014, **44**, 66–69.

5 (*a*) H. Xiong, M. D. Slater, M. Balasubramanian, C. S. Johnson and T. Rajh, Amorphous TiO_2 nanotube anode for rechargeable sodium ion batteries, *J. Phys. Chem. Lett.*, 2011, **2**(20), 2560–2565; (*b*) M. Gu, A. Kushima, Y. Shao, J.-G. Zhang, J. Liu, N. D. Browning, J. Li and C. Wang, Probing the failure mechanism of SnO_2 nanowires for sodium-ion batteries, *Nano Lett.*, 2013, **13**(11), 5203–5211; (*c*) M. Hu, Y. Jiang, W. Sun, H. Wang, C. Jin and M. Yan, Reversible conversion-alloying of Sb_2O_3 as a high-capacity, high-rate, and durable anode for sodium ion batteries, *ACS Appl. Mater. Interfaces*, 2014, **6**(21), 19449–19455; (*d*) G. Grinbom, D. Duveau, G. Gershinsky, L. Monconduit and D. Zitoun, Silicon/Hollow γ-Fe_2O_3 Nanoparticles as Efficient Anodes for Li-Ion Batteries, *Chem. Mater.*, 2015, **27**(7), 2703–2710.

6 J. Qian, Y. Chen, L. Wu, Y. L. Cao, X. P. Ai and H. X. Yang, High capacity Na-storage and superior cyclability of nanocomposite Sb/C anode for Na-ion batteries, *Chem. Commun.*, 2012, **48**, 7070–7072.

7 H. Zhu, Z. Jia, Y. Chen, N. Weadock, J. Wan, O. Vaaland, X. Han, T. Li and L. Hu, Tin anode for sodium-ion batteries using natural wood fiber as a mechanical buffer and electrolyte reservoir, *Nano Lett.*, 2013, **13**(7), 3093–3100.

8 X. Xie, K. Kretschmer, J. Zhang, B. Sun, D. Su and G. Wang, Sn@CNT nanopillars grown perpendicularly on carbon paper: a novel free-standing anode for sodium ion batteries, *Nano Energy*, 2015, **13**, 208–217.

9 H. Hou, Y. Yang, Y. Zhu, M. Jing, C. Pan, L. Fang, W. Song, X. Yang and X. Ji, An Electrochemical Study of Sb/Acetylene Black Composite as Anode for Sodium-Ion Batteries, *Electrochim. Acta*, 2014, **146**, 328–334.

10 L. Wu, H. Lu, L. Xiao, X. Ai, H. Yang and Y. Cao, Electrochemical properties and morphological evolution of pitaya-like Sb@C microspheres as high-performance anode for sodium ion batteries, *J. Mater. Chem. A*, 2015, **3**(10), 5708–5713.

11 (*a*) Y. Kim, Y. Park, A. Choi, N. S. Choi, J. Kim, J. Lee, J. H. Ryu, S. M. Oh and K. T. Lee, An amorphous red phosphorus/carbon composite as a promising anode material for sodium ion batteries, *Adv. Mater.*, 2013, **25**(22), 3045–3049; (*b*) J. Qian, X. Wu, Y. Cao, X. Ai and H. Yang, High capacity and rate capability of amorphous phosphorus for sodium ion batteries, *Angew. Chem.*, 2013, **52**(17), 4633–4636.

12 W. J. Li, S. L. Chou, J. Z. Wang, H. K. Liu and S. X. Dou, Simply mixed commercial red phosphorus and carbon nanotube composite with exceptionally reversible sodium-ion storage, *Nano Lett.*, 2013, **13**(11), 5480–5484.

13 W. J. Li, S. L. Chou, J. Z. Wang, H. K. Liu and S. X. Dou, A new, cheap, and productive FeP anode material for sodium-ion batteries, *Chem. Commun.*, 2015, **51**(17), 3682–3685.

14 (*a*) Y. Kim, Y. Kim, A. Choi, S. Woo, D. Mok, N. S. Choi, Y. S. Jung, J. H. Ryu, S. M. Oh and K. T. Lee, Tin Phosphide as a Promising Anode Material for Na-Ion Batteries, *Adv. Mater.*, 2014, **26**(24), 4139–4144. (*b*) J. Qian, Y. Xiong, Y. Cao, X. Ai and H. Yang, Synergistic Na-Storage Reactions in Sn_4P_3 as a High-Capacity, Cycle-Stable Anode of Na-Ion Batteries, *Nano Lett.*, 2014, **14**, 1865–1869; (*c*) T. Ramireddy, M. M. Rahman, T. Xing, Y. Chen and A. M. Glushenkov, Stable anode performance of an Sb–carbon nanocomposite in lithium-ion batteries and the effect of ball milling mode in the course of its preparation, *J. Mater. Chem. A*, 2014, **2**(12), 4282; (*d*) Z. Zhu, S. Wang, J. Du, Q. Jin, T. Zhang, F. Cheng and J. Chen, Ultrasmall Sn nanoparticles embedded in nitrogen-doped porous carbon as high-performance anode for lithium-ion batteries, *Nano Lett.*, 2013, **14**(1), 153–157.

15 W. Li, S. L. Chou, J. Z. Wang, J. H. Kim, H. K. Liu and S. X. Dou, $Sn_x^{4+}P_3$ @ amorphous Sn–P composites as anodes for sodium-ion batteries with low cost, high capacity, long life, and superior rate capability, *Adv. Mater.*, 2014, **26**(24), 4037–4042.

16 T. H. De Keijser, J. Langford, E. J. Mittemeijer and A. Vogels, Use of the Voigt function in a single-line method for the analysis of X-ray diffraction line broadening, *J. Appl. Crystallogr.*, 1982, **15**(3), 308–314.

17 (*a*) R. Kostecki, B. Schnyder, D. Alliata, X. Song, K. Kinoshita and R. Kötz, Surface studies of carbon films from pyrolyzed photoresist, *Thin Solid Films*, 2001, **396**(1–2), 36–43; (*b*) M. K. Datta, R. Epur, P. Saha, K. Kadakia, S. K. Park and P. N. Kumta, Tin and graphite based nanocomposites: potential anode for sodium ion batteries, *J. Power Source*, 2013, **225**(0), 316–322.

18 J. Sun, G. Zheng, H.-W. Lee, N. Liu, H. Wang, H. Yao, W. Yang and Y. Cui, Formation of Stable Phosphorus–Carbon Bond for Enhanced Performance in Black Phosphorus Nanoparticle–Graphite Composite Battery Anodes, *Nano Lett.*, 2014, **14**(8), 4573–4580.

19 Y. Liu, N. Zhang, L. Jiao, Z. Tao and J. Chen, Ultrasmall Sn Nanoparticles Embedded in Carbon as High-Performance Anode for Sodium-Ion Batteries, *Adv. Funct. Mater.*, 2015, **25**(2), 214–220.